# Accelerated Local Binary Fitting Scheme for Medical Images Segmentation

Mohammad Bagher Khamechian and Mahdi Saadatmand-Tarzjan

**Abstract.** Geometric and geodesic active contours are typical approaches for medical image segmentation. Specially, local binary fitting (LBF) effectively takes advantage of the local intensity average in the energy functional to overcome segmentation difficulties caused by intensity in homogeneity and ruptured edges. Despite promising results, the convergence rate of LBF is too slow. In this paper, we proposed a new efficient implementation of LBF based on the additive operator splitting scheme. In more detail, the multi-dimensional deformation equation of LBF is decomposed into some one-dimensional equations which can be efficiently solved by Tomas' algorithm. Experimental results demonstrated that the proposed algorithm performs better than LBF in terms of both CPU time and solution quality.

**Keywords:** Geometric active contours, level set, local binary fitting, additive operator splitting, image segmentation.

## 1. Introduction

Deformable models are frequently-used and well-known approaches in medical image segmentation. They were primarily introduced by Kass *et al.* [1] based on evolving/deforming a parametric active contour (Snake) in the image domain to minimize the internal and external energy functionals. The former makes the curve smooth while the later moves it toward the interested features in the image domain. In order to handle topological changes and increasing numerical stability, Sethian *et al.* [2,3] proposed geometric active contours based on the level-set function.

Primarily, the edge-based geometric active contours, established by Casllese *et al.* [4,5], Kichenassamy *et al.* [6], and Siddiqi *et al.* [7] effectively employ the object boundary information for segmentation. However, the *active contour without edges* (ACWE) is the first region-based deformable model. It takes advantage of average gray-levels of the internal and external regions of the curve for evolving the active contour based on the Mumford-Shah energy functional [8]. Afterwards, they extended their work for segmentation of the multi-phase homogeneous and inhomogeneous images [9]. Despite significant advantages, both region-based and edge-based deformable models suffer considerable difficulties in segmentation of medical images due to boundary rupturing, gray-level inhomogeneity, and imaging artifacts.

Manuscript received May 24, 2013; revised November 13, 2013; accepted November 27, 2013 .

The authors are with the Department of Electrical Engineering, Ferdowsi University of Mashhad, Iran. The corresponding author's email is: saadatmand@um.ac.ir.

Recently, patch-based deformable models have been proposed as a solution [11-15]. Generally, they effectively employ local edge and region information by taking advantage of appropriate kernel functions. For example, Lankton *et al.* [13] proposed a natural framework that allows any region-based segmentation energy to be re-formulated in a local way. Then, they effectively used the framework with three well-known region-based schemes for segmentation of different medical images. Li *et al.* [14] introduced a patch-based method based on the k-means clustering framework for multi-phase segmentation and bias correction of inhomogeneous medical images. In another work, they presented the local binary fitting (LBF) which employs local intensity average to cope intensity inhomogeneity and ruptured edges. Although LBF provides remarkable results in medical images segmentation, it is afflicted by low convergence rate and sensitivity to parameters, mainly because of using inefficient re-initialization process (in each step, during evolution) and small time-step size (necessary to guarantee the evolution stability).

### *1.1. AOS-Based Implementations*

To speed-up the evolution of active contours, Weickert *et al.* [16] proposed the additive operator splitting (AOS) method. AOS is an efficient numerical framework to accelerate curvature-based methods. They demonstrated that AOS can expedite typical edge-based active contours with the coefficient of 9. The basic idea of AOS is decomposition of a multi-dimensional problem into some one-dimensional sub-problems which can be solved significantly more efficient. The final multi-dimensional solution is approximated as the average of all given one-dimensional solutions.

A number of active contours took advantage of AOS to speed up their implementation. For example, Paragios*et al.* [17] combined the geodesic active contour [4] with the gradient vector flow [18] and utilized AOS for efficient implementation. Goldenberg *et al.* [19] took advantage of both AOS and narrowband technique (NRT) [20] for efficient tracking in color videos. They used the Fast marching method [21] for accelerating the re-initialization of the distance function. Han *et al.* [24] also employed AOS with the geodesic active contour. In another work, Zheng *et al.* [22] improved implementation of the Mumford-Shah energy functional [10] by AOS and NRT methods. Also, Leo *et al.* [23] used Zheng's approach for segmentation of red cells in microscopic images of the urinary sediment. As another example, Jeon *et al.* [25] could successfully speed up ACWE by using AOS for segmentation of multi-phase images.

*1.2. ALBF*

In this paper, we proposed an extended version of AOS for efficient implementation of LBF. It has been successfully used for segmentation of a number of different medical images. In comparison with LBF, the proposed accelerated version of LBF (referred to as ALBF) converged at-least 5 times faster with equivalent solution quality. Furthermore, experimental results demonstrated that compared to ACWE and a frequently-used version of the edge-based geometric active contour, ALBF could superiorly segment the blood-pool boundary of the left ventricle in 11 cardiac magnetic resonance (MR) images in terms of both the area-similarity and shape-similarity measures. The desired boundary of each benchmark image was manually delineated by a cardiologist expert.

*1.3. Paper Outline*

The remainder of the paper is organized as follows. Section 2 briefly presents the LBF scheme. The AOS framework is stated in Section 3. Section 4 is devoted to state the proposed method in detail. Experimental results are given in Section 5 and finally, conclusions are drawn in Section 6.

## 2. Local Binary Fitting Scheme

Let's assume the image $u:\Omega\to R$ with the domain $\Omega\subset R^2$ and gray-level $u(\boldsymbol{x})\in[0,1]$ for all $\boldsymbol{x}=(x,y)\in\Omega$. The energy functional of LBF is given by [11]

$$\begin{aligned} &J(\varphi,f_1,f_2)= \\ &\lambda_1\int_\Omega\int K_\sigma(\mathbf{x}-\mathbf{y})\left|u(\mathbf{y})-f_1(\mathbf{x})\right|^2 M_{1,\varepsilon}(\varphi(\mathbf{y}))d\mathbf{y}d\mathbf{x}+ \\ &\lambda_2\int_\Omega\int K_\sigma(\mathbf{x}-\mathbf{y})\left|u(\mathbf{y})-f_2(\mathbf{x})\right|^2 M_{2,\varepsilon}(\varphi(\mathbf{y}))d\mathbf{y}d\mathbf{x}+ \\ &\upsilon\int\left|\nabla H_\varepsilon(\varphi(\mathbf{x}))\right|d\mathbf{x}+\mu\int\frac{1}{2}\left(\left|\nabla\varphi(\mathbf{x})\right|-1\right)^2 d\mathbf{x}, \end{aligned} \tag{1}$$

where $\phi$ is the level-set function, $\lambda_1,\lambda_2,\upsilon$ and $\mu$ are four constant coefficients, and $\boldsymbol{y}\in\Omega$ represents the neighbors of the central pixel $\boldsymbol{x}$. Also, we have

$$\begin{cases} M_{\varepsilon,1}(\varphi(\mathbf{y}))=H_\varepsilon(\varphi(\mathbf{y})) \\ M_{\varepsilon,2}(\varphi(\mathbf{y}))=1-H_\varepsilon(\varphi(\mathbf{y})), \end{cases} \tag{2}$$

where $H_\varepsilon(\phi)$ is a regularized Heaviside function defined as

$$H_\varepsilon(\varphi)=\frac{1}{2}\left(1+\frac{2}{\pi}\arctan(\frac{\varphi}{\varepsilon})\right). \tag{3}$$

Also, the Gaussian kernel $K_\sigma$ (with the standard deviation of $\sigma>0$) is computed by

$$K_\sigma(\mathrm{u})=\frac{1}{(2\pi)^{n/2}\sigma^n}e^{-|\mathrm{u}|^2/2\sigma^2} \tag{4}$$

In Eq. (1), the functions $f_1(\boldsymbol{x})$ and $f_2(\boldsymbol{x})$ locally approximate $u(\boldsymbol{x})$ in the inside and outside regions of the active contour, respectively. They can be optimally obtained by

$$f_i(\mathbf{x})=\frac{K_\sigma(\mathbf{x})*\left[M_{\varepsilon,i}(\varphi(\mathbf{x}))u(\mathbf{x})\right]}{K_\sigma(\mathbf{x})*M_{\varepsilon,i}(\varphi(\mathbf{x}))} \qquad i=1,2 \tag{5}$$

Finally, according to the Euler-Lagrange equation, LBF evolution equation is given by [11]

$$\begin{aligned} \frac{\partial\varphi}{\partial t}=&-\delta(\varphi)\left(\lambda_1 e_1-\lambda_2 e_2\right)+\nu\,\delta(\varphi)\,\mathrm{div}\left(\frac{\nabla\varphi}{|\nabla\varphi|}\right) \\ &+\mu\left(\nabla^2\varphi-\mathrm{div}\left(\frac{\nabla\varphi}{|\nabla\varphi|}\right)\right), \end{aligned} \tag{6}$$

where $t$ is the time variable, $\delta(\phi)$ denotes the derivative of $H_\varepsilon(\phi)$, and $\nabla$, div, and $\nabla^2$ represent the gradient, divergence and Laplacian operators, respectively. Also, the functions $e_1$ and $e_2$ (given by the Euler-Lagrange equation for the first two terms of Eq. 1) are obtained by

$$\begin{cases} e_1(\mathbf{x})=\int_\Omega K_\sigma(\mathbf{y}-\mathbf{x})\left|u(\mathbf{x})-f_1(\mathbf{y})\right|^2 d\mathbf{y} \\ e_2(\mathbf{x})=\int_\Omega K_\sigma(\mathbf{y}-\mathbf{x})\left|u(\mathbf{x})-f_2(\mathbf{y})\right|^2 d\mathbf{y} \end{cases} \tag{7}$$

In the LBF energy functional (Eq. 1), the first two terms move the active contour toward the desired boundary, the third expression keeps the active contour continuous and derivable, and finally, the last term preserves the distance function ($\phi$) regularity during curve deformation.

## 3. Additive Operator Splitting Scheme

Additive operator splitting (AOS) [16] is an unconditionally stable numerical scheme which presents an efficient approach for solving a curvature-based partial differential equation (PDF). In more detail, typical numerical implementations remain stable only with a small-enough time-step. Thus, they require a large number of iterations for convergence. However, AOS remains stable with a larger time-step size and in sequence, convergence is achieved with fewer iterations.

Let us briefly explain AOS procedure already used to numerically implement the evolution equation of the geometric/geodesic active contours. In more detail, the curvature-based evolution equation of the level-set method is given by

$$\frac{\partial\varphi}{\partial t}=\alpha(\mathbf{x})\,\mathrm{div}\left(\beta(\mathbf{x})\,\frac{\nabla\varphi}{|\nabla\varphi|}\right),\quad \varphi(0)=\varphi_0 \tag{8}$$

where $\alpha$ and $\beta$ are two functions and the level-set function $\phi$ is primarily initialized by $\phi_0$. For example, the above equation with ($\alpha=g$, $\beta=1$) and ($\alpha=1$, $\beta=g$) yields the

geometric and geodesic active contours, respectively, where $g: R^2 \to (0,1]$ is a stopping function (*e.g.*, $g = \frac{1}{1+\left|\nabla(K_\sigma * u)\right|}$).

The explicit scheme is obtained by utilizing the matrix-vector notation for Eq. (8) as

$$\varphi^{n+1} = \varphi^n + \tau \sum_{l=1}^{m} A_l(\varphi^n)\varphi^{n+1} \tag{9}$$

where $l$ is defined to indicate every dimension of the $m$-dimensional coordinates system (e.g. for a 2-D level-set function, we have $m = 2$, $x_1=x$ and $x_2=y$). Also, the superscript $n$ indicates the iteration number (e.g. $\phi^0=\phi_0$), $I$ denotes the unit matrix, $\tau$ is the time-step size, and $A_l(\phi^n) = [\hat{a}_{ijl}(\phi^n)]$ is an operator matrix which indicates the interaction along the $l$-th direction; such that

$$\hat{a}_{ijl}(\varphi^n) = \begin{cases} \dfrac{2\alpha_i}{\left(\dfrac{|\nabla\varphi|}{\beta}\right)_i^n + \left(\dfrac{|\nabla\varphi|}{\beta}\right)_j^n} & j \in N_l(i) \\ -\alpha_i \sum\limits_{m \in N_l(i)} \dfrac{2}{\left(\dfrac{|\nabla\varphi|}{\beta}\right)_i^n + \left(\dfrac{|\nabla\varphi|}{\beta}\right)_m^n} & j = i \\ 0 & \text{Otherwise} \end{cases} \tag{10}$$

where the set $N_l(i)$ includes two neighboring pixels of the $i$-th pixel along the $l$-th direction. However, the explicit scheme requires a small $\tau$ for robust convergence.

On the other hand, for solving Eq. (8), we can employ the semi-implicit scheme as

$$\varphi^{n+1} = \left[I - \tau \sum_{l=1}^{m} A_l(\varphi^n)\right]^{-1} \varphi^n \tag{11}$$

Although the semi-implicit scheme is unconditionally stable, inverting the large bandwidth matrix requires immense computational burden. To tackle this problem, we may take advantage of the AOS variant given by

$$\varphi^{n+1} = \frac{1}{m}\sum_{l=1}^{m}\left[I - \tau\, m\, A_l(\varphi^n)\right]^{-1}\varphi^n \tag{12}$$

The above equation, which provides a solution to Eq. (8), can be efficiently implemented by Tomas' algorithm [16].

## 4. Proposed Algorithm

As aforementioned, the convergence rate of LBF is restricted by the time-step size. This difficulty can be addressed by utilizing AOS scheme in numerical implementation.

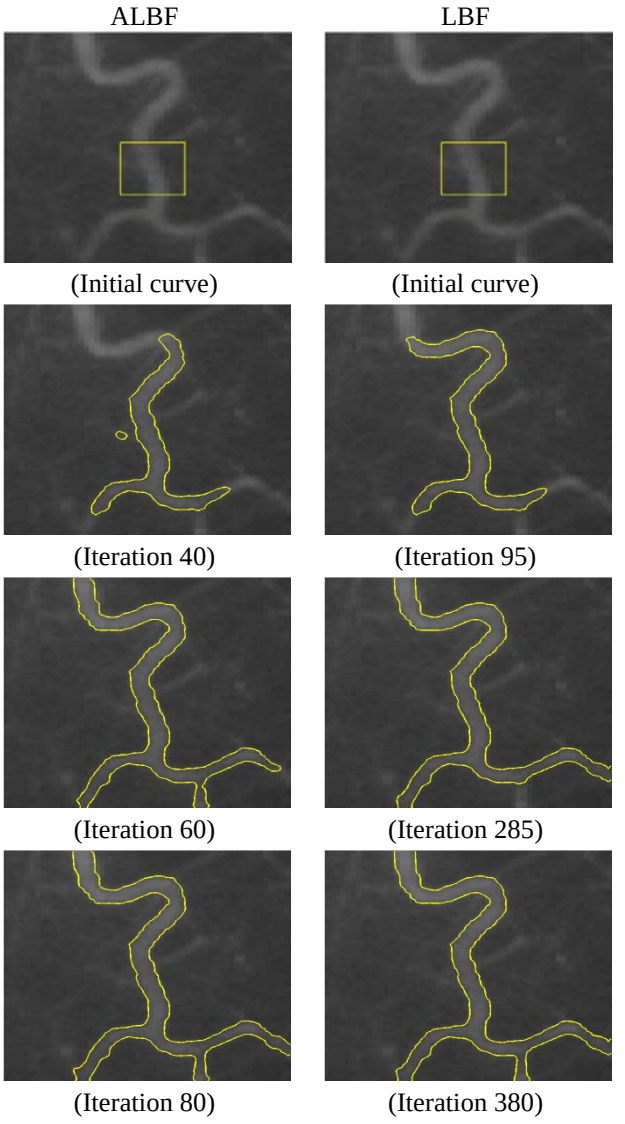


Fig. 1. Comparing the convergence rate of (left column) ALBF and (right column) LBF for the image *vessel* (of size 111×110). The corresponding iteration number is quoted under each illustration.

The general deformation PDE of an active contour can be usually written as follows:

$$\frac{\partial\varphi}{\partial t} = \alpha\ \mathrm{div}\left(\beta\ \frac{\nabla\varphi}{|\nabla\varphi|}\right) + E, \tag{13}$$

where the speed $E$ is typically obtained from the external and regularization terms of the energy functional. In this case, the AOS scheme can be simply extended to

$$\varphi^{n+1} = \frac{1}{m}\sum_{l=1}^{m}\left[I - \tau\, m\, A_l(\varphi^n)\right]^{-1}\left(\varphi^n + \tau\, E\right). \tag{14}$$

Specially, we can rewrite the deformation equation of LBF (Eq. 6) in the form of Eq. (13) by using

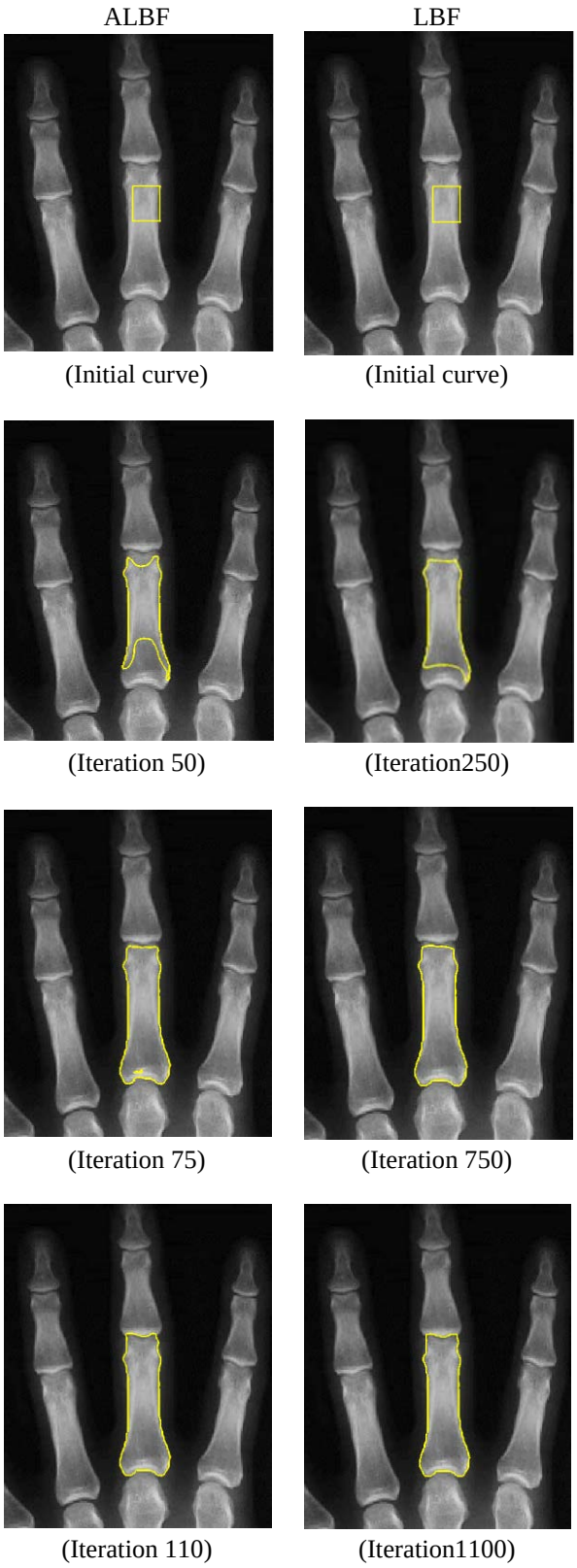


Fig. 2. Comparing the convergence rate of (left column) ALBF and (right column) LBF for the image *finger bone* (of size 236×213).

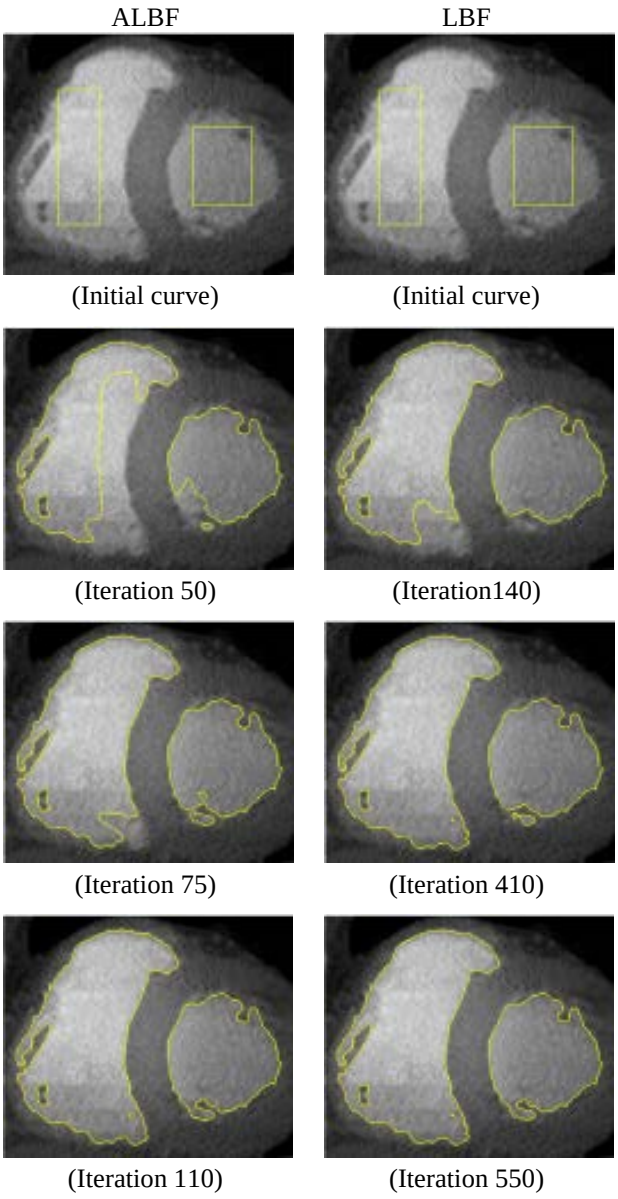


Fig. 3. Comparing the convergence rateof (left column) ALBF and (right column) LBF for the image heart (of size 152×128).

$$\begin{cases} \alpha = v\delta(\varphi) - \mu \\ \beta = 1 \\ E = \mu\nabla^2\varphi - \delta(\varphi)\,(\lambda_1 e_1 - \lambda_2 e_2) \end{cases} \tag{15}$$

Therefore, the AOS scheme of LBF (referred to as ALBF) is computed by

$$\varphi^{n+1} = \frac{1}{m}\sum_{l=1}^{m}\left[I - \tau m A_l(\varphi^n)\right]^{-1} \times\left[\varphi^n + \tau\left(\mu\nabla^2\varphi - \delta(\varphi)\,(\lambda_1 e_1 - \lambda_2 e_2)\right)\right] \tag{16}$$

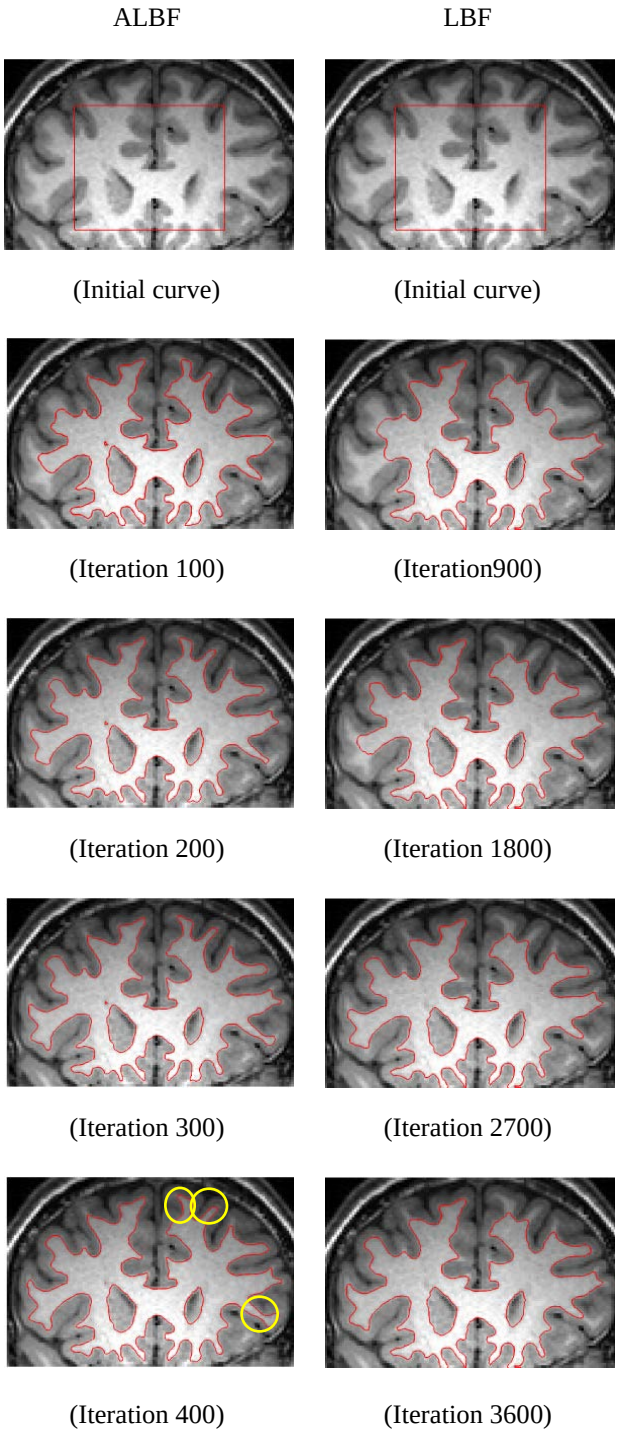


Fig. 4. Comparing the convergence rateof (left column) ALBF and (right column) LBF for the image *brain* (of size 119×78).

### *4.1. Implementation*

In the 2D case (*i.e.* $m$=2), each deformation step of ALBF (Eq. 16) consists of four stages

*i)* Computation of $\Phi^n$ as follows

$$\Phi^n = \varphi^n + \tau\left(\mu\nabla^2\varphi - \delta(\varphi)\,(\lambda_1 e_1 - \lambda_2 e_2)\right) \qquad (17)$$

*ii)* Evolution along the $x_1$=$x$ direction by solving the following tri-diagonal set of equations using Tomas' algorithm to obtain $v^{n+1}$

$$[I - 2\tau A_x(\Phi^n)]\,v^{n+1} = \Phi^n \qquad (18)$$

*iii)* Similarly, evolution along the $x_1$=$y$ direction to obtain $u^{n+1}$

$$[I - 2\tau A_x(\Phi^n)]\,u^{n+1} = \Phi^n \qquad (19)$$

*iv)* Computation of $\phi^{n+1}$ by averaging on $v^{n+1}$ and $u^{n+1}$, given by

$$\varphi^{n+1} = \frac{1}{2}(u^{n+1} + v^{n+1}) \qquad (20)$$

Table 1. Comparing CPU-times of ALBF and LBF for four benchmark medical images.

| | **ALBF** | | **LBF** | |
|---|---|---|---|---|
| | **CPU Time (s)** | **Iterations Number** | **CPU Time (s)** | **Iterations Number** |
| Vessel | 1.28 | 80 | 2.77 | 380 |
| Finger bone | 3.35 | 110 | 13.19 | 1100 |
| Heart | 2.27 | 110 | 6.56 | 550 |
| Brain | 3.78 | 400 | 19.57 | 3600 |

## 5. Experimental Results

The performance of ALBF was compared with that of LBF by using four medical benchmark images including *vessel* (an angiographic image), *finger bone* (a radiology image), *heart* (a cardiac CT image), and *brain* (a MR image of the brain white matter of the human). All the experimental results were obtained by a LAPTOP with CPU Core-i5 3.2GHz and 1-GB main memory using MATLAB environment. Furthermore, in each experiment, the same parameters values were chosen for the both counterpart methods.

The deformation process of LBF and ALBF for all benchmark images are illustrated in Figs. 1-4. In every figure, for each algorithm, some illustrations of middle steps of the deformation process are appeared (the corresponding iteration number is quoted under each illustration).

As shown, for all benchmark images, the number of iterations necessary for LBF convergence was, at least, 5 times greater than that of ALBF. It is further illustrated in Table 1 which includes CPU times. For all benchmark images, ALBF was converged above twice faster compared to LBF. For example, for the Brain image, the CPU times of LBF and ALBF were 19.57 and 3.78 seconds, respectively.

Although the solutions of LBF and ALBF were similar in all experiments, ALBF slightly perform better to segment thin structures in the image. For example, as illustrated in Fig. 4, ALBF could better segment narrow cavities of the

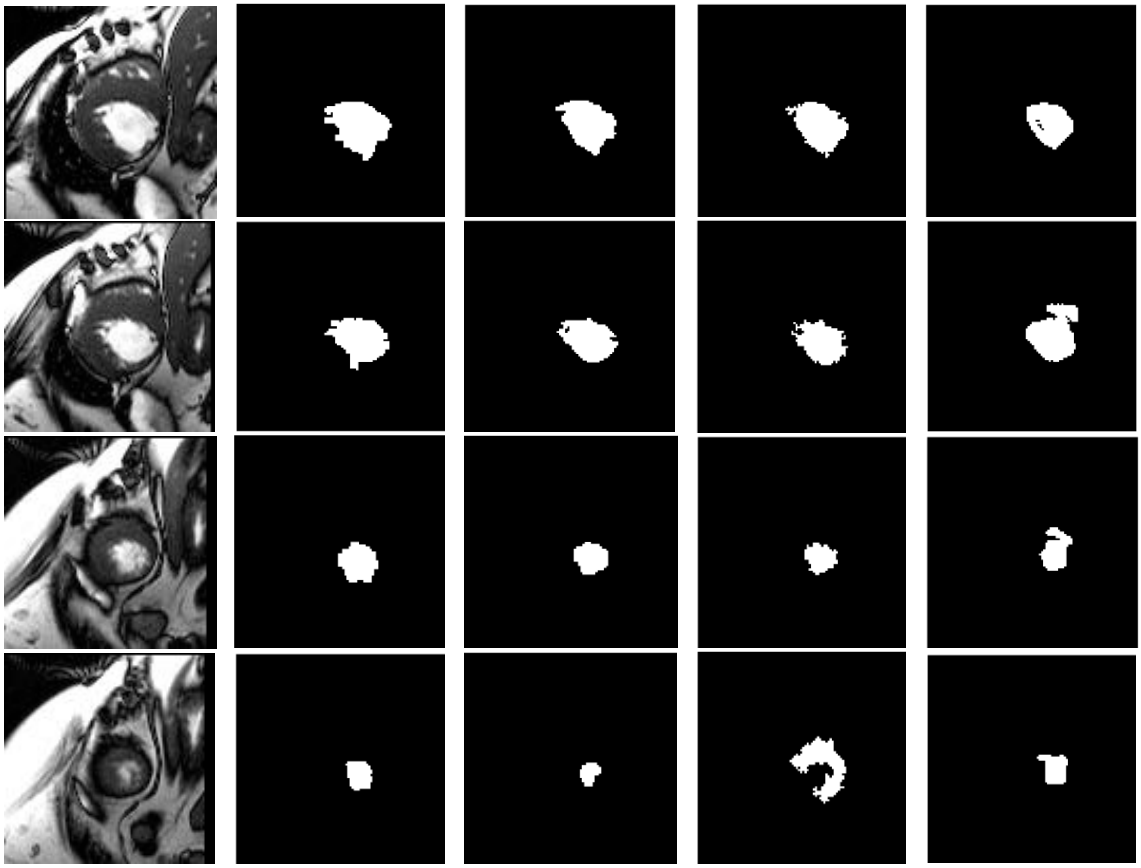


Fig. 5. Comparing the results of ALBF, ACWE and GCM with the desired boundary manually delineated by a cardiologist expert for four different CMR images.

brain white-matter (shown by yellow ellipses) compared to LBF. In other words, ALBF overcame LBF in terms of both CPU time and (slightly) solution quality.

### *5.1. Solution Quality Evaluations*

To further evaluate the solution quality of ALBF, 11 different gradient-echo cardiac MR (CMR) images (obtained by a 1.5-Tesla MR scanner) were used for the blood-pool boundary segmentation. The desired boundary of each benchmark image was manually delineated by a cardiologist expert. In Fig. 5, the solutions of ALBF are compared with those of ACWE [8] and a well-known frequently-used version of the edge-based geometric active contour (GAC) [26, 27] for 4 different CMR images. Obviously, ALBF provided the best results for all benchmark images.

For further quantitative comparisons, we used the average area-similarity ($S_{\text{area}}$) and shape-similarity ($S_{\text{shape}}$) measures for all the benchmark images. In more detail, the area-similarity measure ($S_{\text{area}} \in [0,1]$) compares the blood-pool region ($A_1$) obtained by the algorithm with the manually delineated area ($A_2$), as follows:

$$S_{\text{area}} = \frac{2\, n(A_1 \cap A_2)}{n(A_1) + n(A_2)} \tag{21}$$

where $n(.)$ returns the number of pixels in a region. Since $S_{\text{area}}$ cannot effectively evaluate the similarity of the resultant boundaries, we also used the shape-similarity measure, primarily proposed by Pluempitiwiriyawej *et al.* [28]. For two completely matched boundaries, $S_{\text{shape}}$ results to 1 while it decreases to 0 in the worst case.

The evaluation results are presented in Table 2. As shown ALBF provided superior solution quality compared to ACWE and GAC in term of both the average area-similarity and shape-similarity measures.

Table 2. Comparing the results of ALBF, ACWE, and GAC in terms of the average area-similarity and shape-similarity measures for 11 CMR images. The standard deviations are quoted inside the brackets. Also, the best results are indicated by bold-faced text.

| **Method** | $\boldsymbol{S}_{\textbf{area}}$ | $\boldsymbol{S}_{\textbf{shape}}$ |
|---|---|---|
| ALBF | 0.85 [0.08] | 0.9 [0.03] |
| ACWE | 0.72 [0.29] | 0.75 [0.17] |
| GAC | 0.69 [0.12] | 0.59 [0.11] |

## 6. Conclusion

Although LBF can be used for segmentation of images with intensity inhomogeneity and ruptured edges, it suffers from slow deformation convergence. In this paper, we proposed an efficient variant of LBF based on the AOS method. Indeed, instead of the explicit implementation, we solved PDE of the LBF energy functional by using the AOS scheme. It equivalently decomposes a multi-dimensional spatial operator into some one-dimensional operators which can be separately solved by the efficient Thomas' algorithm. The experimental results demonstrated that ALBF performs superior to LBF in terms of both CPU-time and (slightly) solution quality. Furthermore, it provided better results for segmentation of the blood-pool of the left ventricle in CMR images compared to ACWE and GAC in terms of both the average area-similarity and shape-similarity measures.

## Acknowledgment

The authors would like to acknowledge the generous support of the Ferdowsi University of Mashhad under the Research Project No. 1/28384.

## References

[1] M. Kass, "Snakes: active countor models," *Int'l Jornal of Computer Vision* , vol. 1, no. 4, pp. 321–331, 1988.

[2] S. Osher and J. A. Sethian, "Fronts propagating with curvature dependent speed: algorithms based on Hamiton-Jacobi formulations," *Journal of Computational Physics*, vol. 79, no. 1, pp. 12–49, 1988.

[3] S. Osher and R. Fedkiw, *Level Set Methods and Dynamic Implicit Surfaces*. Springer-Verlag, 2002.

[4] V. Caselles, R. Kimmel, and G. Sapiro, "Geodesic active contours," in *Proc. IEEE Int'l Conf. Computer Vision*, pp. 694-699, 1995.

[5] V. Caselles, R. Kimmel, and G. Sapiro, "On geodesic active contours," *Int'l J. Computer Vission*, vol. 22, no. 1, pp. 61–79, 1997.

[6] S. Kichenassamy, A. Kumar, P. Olver, A. Tannenbaum, and A. Yezzi, "Conformal curvatures flows: from phase transitions to active vision," *Arch. Rational Mech. Anal.*, vol. 134, no. 3, pp. 275–301, 1996.

[7] K. Siddiqi, Y. B. Lauriere, A. Tannenbaum, and S. W. Zucker, "Areaand length minimizing flows for shape segmentation," *IEEE Trans. Image Processing*, vol. 7, no. 3, pp. 433–443, 1998.

[8] T. Chan and L. Vese, "Active contours without edges," *IEEE Trans. Image Processing*, vol. 10, no. 2, pp. 266–277, 2001.

[9] L. Vese and T. Chan, "A multiphase level set framework for image segmentation using the Mumford and Shah model," *Int'l. J. Computer Vision*, vol. 50, no. 2, pp. 271–293, 2002.

[10] D. Mumford and J. Shah, "Optimal approximations by piecewise smooth functions and associated variational problems," *Communications on Pure and Applied Mathematics*, vol. 42, no. 5, pp. 577–685, 1989.

[11] C. Li, C. Kao, J. Gore, and Z. Ding, "Minimization of region-scalable fitting energy for image segmentation," *IEEE Trans. Image Processing*, vol. 17, no. 10, pp. 1940–1949, 2008.

[12] K. Zhang, "Active contours driven by local image fitting energy," *Pattern Recognition*, vol. 43, no. 4, pp. 1199–1206, 2010.

[13] S. Lankton and A. Tannenbaum, "Localizing region-based active contours," *IEEE Trans Image Processing*, vol. 17, no. 11, pp. 2029–2039, 2008.

[14] C. Li, C-Y. Kao, J. C. Gore, and Z. Ding, "A level set method for image segmentation in the presence of intensity inhomogeneities with application to MRI," *IEEE Trans. Image Processing*, vol. 20, no. 7, pp. 2007–2016, 2011.

[15] J. Yuan, P. Li, Y. Wen, and Y. Xu, "Level set segmentation of intensity inhomogeneous images based on local linear approximation of difference image," *IET Image Processing*, vol. 6, no. 5, pp. 473–482, 2012.

[16] J. Weickert and G. Kuhne, "Fast methods for implicit active contour models," *in Geometric Level Set Methods in Imaging, Vision and Graphics.* S. Osher and N. Paragios, editors, Springer, 2002.

[17] N. Paragios, O. M. Gottardo, and V. Ramesh, "Gradient vector flow fast geodesic active contours," *IEEE Int'l Conf. Computer Vision*, vol. 1, pp. 67–73, 2001.

[18] C. Xu and J. Prince, "Gradient vector flow: a new external force for snakes," *IEEE Conf. Comp. Vis. Patt. Recog.*, pp. 66–71, 1997.

[19] R. Goldenberg, R. Kimmel, E. Rivlin, and M. Rudzsky, "Fast geodesic active contours," *IEEE Trans. Image Processing*, vol. 10, no. 10, pp. 1467–1475, 2001.

[20] D. Adalsteinsson and J. A. Sethian, "A fast level set method for propagating interfaces," *J. Comput. Phys.*, vol. 118, no. 2, pp. 269–277, 1995.

[21] J. A. Sethian, "Level set methods: evolving interfaces in geometry fluid mechanics," in *Computer Vision and Materials Sciences*. Cambridge University Press, 1996.

[22] W. Zheng, Y. Xin, S. Pengfei, "Solving Mumford-Shah model equation by AOS algorithm," *IEEE Int. Conf. Signal Processing*, vol. 1, pp. 740–743, 2002.

[23] H. Luo, S. Ma, D. Wu and Z. Xu, "Mumford-Shah segmentation for microscopic image of the urinary sediment," *IEEE Int'l Conf. Bioinformatics and Biomedical Engineering*, pp. 861–863, 2007.

[24] Z. Han and X. Liu, "An addtive operator splitting method for microscopic image segmentation," *IEEE. Int'l. Conf. Bioinformatics and Biomedical Engineering*, pp. 1–4, 2010.

[25] M. Jeon, M. Alexander, N. Pizzi, and W. Pedrycz, "Unsupervised hierarchical multi-scale image segmentation level set, wavelet and additive splitting operator," *IEEE Annual Meeting of the Fuzzy Information*, vol. 2, pp. 664–668, 2004.

[26] J. Cheng, M. Ding and X. Zhang, "Geometric active contour model and its application to carotid plaque detection," *IEEE*

*Inte'l Conf. Intelligent Computation and Bio-Medical Instrumentation*, pp. 101-104, 2011.

[27] M. Airouche, L. Bentabet and M. Zelmat, "Image segmentation using active contour model and level set method applied to detect oil spills," *Proc. of the World Congress on Engineering*, vol. 1, London, 2009.

[28] C. Pluempitiwiriyawej, J. M. F. Moura, Y.-J. Lin Wu, and C. Ho, "STACS: New active contour scheme for cardiac MR image segmentation," *IEEE Trans. Medical Imaging*, vol. 24, no. 5, pp. 593–603, 2005.

**Mohammad Bagher Khamechian** received the B.S. and M.S. degrees in biomedical engineering from Azad University and Ferdowsi University of Mashhad, Mashhad, Iran, in 2011 and 2014, respectively. He is currently working toward the Ph.D. degree in biomedical engineering at University of Science and Technology, Tehran, Iran. His research interests include medical image processing, medical imaging, biomedical signal analyzing, and cognitive systems.

**Mahdi Saadatmand-Tarzjan** received the B.S. degree in electrical (control) engineering from the Ferdowsi University of Mashhad (Mashhad, Iran) in 2002, and the M.S. and Ph.D. degrees, both in biomedical engineering, from the K. N. Toosi University of Technology (Tehran, Iran) and Tarbiat-Modares University (Tehran, Iran) in 2005 and 2010, respectively.

His research interests include medical imaging, medical image processing, machine vision, and soft computing of which he has published more than 70 peer-reviewed articles.

Dr. Saadatmand-Tarzjan is the recipient of several awards including the Outstanding Undergraduate Student Award (2003), two Khawrazmi Youth Festival Awards (2003 and 2004), Outstanding Graduate Researcher Award (2004), and the educational fund award of the National Youth Foundation (2008). Since 2011, he has worked as Assistant Professor at the Department of Electrical (Biomedical) Engineering of the Ferdowsi University of Mashhad (Mashhad, Iran).